Published in final edited form as:
Biomaterials. 2014 December ; 35(38): 10015–10024. doi:10.1016/j.biomaterials.2014.08.047.

Micro-scale and meso-scale architectural cues cooperate and compete to direct aligned tissue formation

Christopher L. Gilchrist[a], **David S. Ruch**[a], **Dianne Little**[a], and **Farshid Guilak**[a,b,*]

[a]Department of Orthopaedic Surgery, Duke University Medical Center, Durham, NC 27710, USA

[b]Department of Biomedical Engineering, Duke University, Durham, NC 27708, USA

Abstract

Tissue and biomaterial microenvironments provide architectural cues that direct important cell behaviors including cell shape, alignment, migration, and resulting tissue formation. These architectural features may be presented to cells across multiple length scales, from nanometers to millimeters in size. In this study, we examined how architectural cues at two distinctly different length scales, “micro-scale” cues on the order of ~1–2 μm, and “meso-scale” cues several orders of magnitude larger (>100 μm), interact to direct aligned neo-tissue formation. Utilizing a micro-photopatterning (μPP) model system to precisely arrange cell-adhesive patterns, we examined the effects of substrate architecture at these length scales on human mesenchymal stem cell (hMSC) organization, gene expression, and fibrillar collagen deposition. Both micro- and meso-scale architectures directed cell alignment and resulting tissue organization, and when combined, meso cues could enhance or compete against micro-scale cues. As meso boundary aspect ratios were increased, meso-scale cues overrode micro-scale cues and controlled tissue alignment, with a characteristic critical width (~500 μm) similar to boundary dimensions that exist *in vivo* in highly aligned tissues. Meso-scale cues acted via both lateral confinement (in a cell-density-dependent manner) and by permitting end-to-end cell arrangements that yielded greater fibrillar collagen deposition. Despite large differences in fibrillar collagen content and organization between μPP architectural conditions, these changes did not correspond with changes in gene expression of key matrix or tendon-related genes. These findings highlight the complex interplay between geometric cues at multiple length scales and may have implications for tissue engineering strategies, where scaffold designs that incorporate cues at multiple length scales could improve neo-tissue organization and resulting functional outcomes.

Keywords

Micropatterning; Actin; Tendon; Nanotopography; Mesenchymal stem cell; Ligament

*Corresponding author. Department of Orthopaedic Surgery, Duke University Medical Center, MSRB 375, Box 3093, Durham, NC 27710, USA. Fax: +1 919 681 8490. guilak@duke.edu. .

Appendix A. Supplementary data Supplementary data related to this article can be found at http://dx.doi.org/10.1016/j.biomaterials.2014.08.047.

1. Introduction

Cellular organization and alignment play key roles in determining tissue formation and function across a wide range of tissues, contributing to both biological and mechanical functions of a tissue. For example, during development of collagenous tissues such as tendon [1] cells become highly aligned and assemble a dense, extremely ordered collagen fiber extracellular matrix that is critical to the tissue's function of resisting tensile mechanical loads. An important factor driving cell organization and alignment behaviors during neo-tissue formation is the extracellular microenvironment within which cells reside. In addition to soluble mediators such as growth factors, physical signals such as tissue stiffness, topography and geometry, and extracellular matrix (ECM) ligands have been shown to affect and direct a wide variety of cell behaviors including migration, shape, aggregation, and differentiation (reviewed in [Refs. 2,3]). During tissue development, these cues are often presented to cells in complex combinations with spatial and temporal gradients that may be distributed across different length scales. For tissue engineering applications, biomaterial scaffolds that present specific microenvironmental cues (e.g., nano- and micro-topography, cell-adhesive ligands, growth factor gradients) to cells have shown considerable promise for locally guiding cell organization, phenotype, and resulting tissue formation [4-11]. However, relatively little is known about how combinations of these cues interact to precisely control cell and tissue organization.

Tissue architecture is one important category of microenvironmental cue that, via contact guidance [12,13] or cell confinement (i.e., tissue geometrical constraint) [14,15] mechanisms, direct a variety of cell behaviors. These cues may occur across a wide range of length scales, from nanometers to millimeters in size. At the nano- and micro-scales, topographies such as fibers, grooves, and pits have been shown to direct cell behaviors including adhesion, shape, survival, focal adhesion and cytoskeletal architecture, gene expression, and stem cell differentiation [16-24]. These cues have been utilized for tissue engineering applications, where, for example, aligned nanofiber scaffolds promote aligned cell morphologies, matrix organization, and tendon-specific cell differentiation [25-28]. Additionally, tissue microenvironments may also include larger meso-scale (hundreds to thousands of microns) geometrical constraints that impose confinement boundary conditions on multicellular cultures, yielding emergent, spatially varying patterns of cell proliferation, growth, differentiation, mechanotransduction, and organization within developing neo-tissues [8,29-34].

Although cells likely experience multi-scale combinations of architectural cues simultaneously *in vivo* and in biomaterial scaffolds, there has been limited work examining how architectural cues from different length scales interact to influence cell behaviors. Several recent studies have investigated the effects of combining aligned topographical cues at nano- and micro-scales on the alignment of single cells, with findings suggesting that cell alignment can be controlled by nano-cues [35,36] or micro-cues [37], and enhanced when cues at both length scales are aligned [38]. However, each of these studies has examined the response of single cells to just one combination of nano/micro-cues (one set of cue geometries arranged in parallel or opposition), and without exploration of downstream behaviors of complex multicellular systems such as tissue assembly or gene expression.

Thus, there remains an incomplete understanding of how cues at different length scales, potentially acting through different mechanisms (contact guidance versus multicellular geometric confinement), combine or interact to direct cell and resulting tissue organization.

The objective of this study was to examine how microenvironment architectural cues at two distinctly different length scales, “micro-scale” cues on the order of ~1–2 μm, and “meso-scale” cues approximately two orders of magnitude larger (>100 μm), combine and interact to direct aligned neo-tissue formation. Using a micro-photopatterning (μPP) system to mimic architectural features of native fibrillar matrices and electrospun fiber scaffolds, cell-adhesive cues at micro and meso-scales were precisely arranged in a variety of combinations, and the effects on human mesenchymal stem cell (hMSC) organization and aligned collagen fibril assembly were examined. Our findings identify a complex interplay between cues at different length scales and illustrate how these cues may cooperate or compete (depending upon their arrangement) to direct the formation and maintenance of aligned tissues.

2. Materials and methods

2.1. Microphotopatterning (μPP)

Cell-adhesive patterns were created within a non-fouling hydrogel layer [39]. Glass-bottomed cover dishes (MatTek Corp) were amino-silanated (1% (3-aminopropyl)trimethoxysilane, Sigma), activated with 0.5% glutaraldehyde, and spin-coated with polyvinyl alcohol (Sigma, 5.6% w/v in 0.2 N HCl) to create a thin (~150 nm thick) hydrogel layer that resists protein adsorption and cell adhesion (stable for >1 month in culture). Cell-adhesive regions within the gel layer were created via photoablation using a two-photon microscope (Olympus FV1000, 25X 1.05NA objective, Ex: 725 nm), and functionalized with fibronectin (20 μg/mL in PBS with 0.1% pluronic F127, Sigma, followed by blocking with 1% heat-denatured BSA, Life Technologies) to promote cell adhesion. For this study, three “micro-scale” μPP cell-adhesive architectures were investigated: *aligned* 2.03 ± 0.05 μm parallel lines spaced 5 μm on center; feature size measured by staining non-ablated regions with Hoechst 33342 (Sigma) and imaging (Zeiss LSM 510, 63X 1.2NA), measurements in FIJI (NIH), $n = 156$), *grid* (lines of same dimensions added in orthogonal direction), and *unpatterned* (fully-ablated). Additionally, the “meso-scale” pattern boundary dimensions were also varied as described below.

2.2. Cell culture

Human mesenchymal stem cells (hMSCs) isolated from bone marrow aspirates (cells pooled from 3 de-identified donors, surgical waste approved as exempt from review by Duke University Institutional Review Board) were expanded in monolayer (passage 5) and seeded onto μPP substrates (1000 cells/cm^2 for single cell experiments, 18,000 cells/cm^2 for all other experiments) with unattached cells removed via media wash. Cells were cultured (5% CO_2, 37 °C) on patterns in culture media (Advanced DMEM, Life Technologies) with 10% FBS, 200 μM L-ascorbic acid 2-phosphate, 2 mM L-glutamine, and 1% penicillin-streptomycin) for either 2 h (single cell experiments) or 3–12 days (all other experiments), then fixed (4% formaldehyde, Electron Microscopy Sciences) for analysis.

2.3. Cell imaging and analysis

Fixed cell constructs were permeabilized (0.1% Triton X-100, 2 min), fluorescently labeled for actin cytoskeleton (Alexa 488 or 633 phalloidin, Life Technologies) and cell nuclei (Hoechst 33342, Life Technologies), and imaged via confocal microscopy (Zeiss LSM 510, 40X 0.95NA). Image stacks were acquired over a depth of 4 μm above the pattern surface to isolate behaviors near the cell–pattern interface. Cell nuclear aspect ratios and nuclear alignment with pattern direction were determined using FIJI's (NIH) best-fit ellipse tool. For single cell experiments, Feret diameters (max, min caliper distances) for cells not in contact with other cells were measured from actin images (FIJI) and used to calculate cell elongation ($Feret_{max}/Feret_{min}$) and alignment ($Feret_{max}$ orientation relative to pattern). Orientation of cell sheets was determined from actin images using fast-fourier transform (FFT) analysis (FIJI Directionality tool), with pixel intensities summed at 2° increments over the power spectrum (−90°–+90°) to generate alignment histograms [40,41]. In cases where overall pattern dimensions were larger than a single image field, tiled images were stitched (FIJI Grid Stitching [42]) prior to FFT analysis. An image's degree of alignment was quantified by calculating the Alignment Index (AI) [40] using Equation (1), where θ_m is the mode of the FFT histogram and I is pixel intensity. In some cases (where specified), the AI was calculated about the μPP pattern direction instead of the histogram mode.

$$\mathbf{AI}=\frac{\int_{\theta_m-20^\circ}^{\theta_m+20^\circ}\boldsymbol{I}\partial\theta}{(40^\circ/180^\circ)\times\int_{-90^\circ}^{90^\circ}\boldsymbol{I}\partial\theta} \quad (1)$$

2.4. Fibrillar collagen imaging and analysis

Fibrillar collagen organization was assessed using both polarized light microscopy and second-harmonic generation (SHG) imaging. For polarized light analysis, samples were stained with picrosirius red (ScyTek) to enhance collagen birefringence and imaged using a polarized light microscope (Olympus E600) equipped with rotating polarizer/analyzer (images acquired at 10° increments; mean pixel intensity over entire μPP pattern area measured for each sample). To detect collagen alignment for a given pattern architecture, differences between mean pattern intensities with polarizer angle were tested (repeated measures ANOVA). To detect differences between pattern architectures, mean pattern intensities at a given polarizer angle were compared (*t*-test). Bonferroni corrections were made for multiple comparisons. SHG image stacks of samples (2 μm deep, starting just above pattern surface) were acquired using a two-photon microscope (Olympus FV1000, 25X objective, Ex/Em:880/440 nm). Directionality of SHG images was analyzed via FFT as described above, with image AI calculated about the histogram mode or pattern orientation.

2.5. Gene expression

Total RNA was extracted from cells grown on μPP patterns following 6 and 12 days of culture (RNeasy Micro kit, Qiagen), and RNA from each sample quantified (Nanodrop ND-1000, Nanodrop Technologies). Equal amounts of RNA were reverse transcribed (Superscript VILO cDNA Synthesis Kit, Life Technologies), and Real Time PCR performed (One Step Plus, Applied Biosystems; Express qPCR SuperMix, Life Technologies).

Transcript levels for genes relating to tendon (collagen types I, III, tenomodulin, tenascin-C) were corrected for reaction efficiency, normalized to GAPDH (endogenous control), then expressed as fold-change relative to hMSCs prior to cell seeding (Day 0). Commercially available primers and probes (Applied Bio-systems) were used to compare transcript levels: type I collagen (COL1A1, assay ID Hs00164004_m1), type III collagen (COL3A1, assay ID Hs00164103_m1), tenascin-C (TNC, assay ID Hs00233648_m1), scleraxis (SCX, assay ID Hs03054634_g1), GAPDH glyceraldehyde-3-phosphate dehydrogenase (GAPDH, endogenous control, assay ID Hs02758991_g1).

2.6. Statistical analyses

All data presented as mean ± standard error. Significance for analysis of variance (ANOVA) analyses detected via Tukey's HSD post hoc test unless otherwise noted. Histograms were compared via Kolmogorov–Smirnov test. Significance of all statistical analyses is reported at the 95% confidence level ($\alpha = 0.05$).

3. Results

3.1. Micro-scale μPP architecture directs cell and matrix organization

Single hMSCs attaching to aligned micro-scale μPP architecture (2 h post-seeding) became highly elongated and aligned with the pattern direction (Fig. 1A and B), whereas cells on either gridded or unpatterned μPP substrates showed significantly less elongation (<50% of cells on aligned patterns, Fig. 1B, $p < 0.0001$) and no alignment preference (Fig. 1C). Similarly, nuclei of single cells on aligned patterns were found to have higher aspect ratios (Fig. 1B, $p < 0.01$) than on other patterns and were aligned with the pattern direction (Fig. 1D), while gridded and unpatterned substrates showed no nuclear alignment preference. To examine the effect of micro-scale architecture on groups of cells, hMSCs were seeded at higher densities (18,000 cells/cm^2) on μPP architectures (aligned, grid, or unpatterned micro-pattern) with square meso-scale boundaries (250 μm × 250 μm, Fig. 2A) and cultured for 12 days to allow for assembly of a fibrillar collagen matrix. Under these conditions, hMSCs grown on aligned μPP substrates exhibited an actin cytoskeleton that was oriented in the pattern direction (Fig. 2B,C) and had significantly greater cytoskeletal alignment (quantified as alignment index (AI), Fig 2C) as compared to cells on grid μPP substrates. Cells on unpatterned substrates exhibited an intermediate AI (Fig. 2C) due to some alignment of cell aggregates in random directions, but on average showed no preferred orientation (Fig. 2C left, FFT intensity plot). Cell nuclear aspect ratios (Fig. 2D) showed similar findings, with highest nuclear elongation on aligned micro-patterns. Additionally, the quantity and alignment of fibrillar collagen matrix produced by hMSCs cultured on μPP architectures was assessed using polarized light (Fig. 2E) and SHG (not shown) imaging. Significant changes in polarized light intensities with polarizer angle were detected for aligned patterns (Fig. 2F), but not for grid or unpatterned substrates, demonstrating that aligned μPP architecture promoted deposition of aligned fibrillar collagen. FFT analysis of SHG images confirmed fibrillar collagen was oriented along the pattern direction (Fig. 2G), with significantly greater AI for aligned architecture as compared to grid and unpatterned substrates (30%–49% AI increase over grid and unpatterned, respectively; $p < 0.04$, Fig. 2G). Together, these findings demonstrate that micro-scale μPP architectural cues have a

significant effect on the organization of single and groups of hMSCs, and direct hMSC fibrillar collagen deposition and organization.

3.2. Meso-scale architecture combines with micro-scale architecture to enhance cell and matrix organization

We next investigated how the meso-scale boundary dimensions of μPP substrates influence cell and matrix organization when combined with micro-scale cues. When hMSCs were seeded onto μPP substrates featuring meso-scale boundaries elongated in the same direction as aligned micro-scale cues (Fig. 3A; 1250 μm × 125 μm boundary dimensions, 10:1 aspect ratio), cell organization was dramatically enhanced relative to square patterns (250 μm × 250 μm, 1:1 aspect ratio). As shown in Fig. 3B, on elongated (10:1) patterns hMSC actin cytoskeleton was highly aligned with the pattern direction, with AI levels 1.6-fold greater than cells square (1:1) patterns with aligned micro-scale cues ($p = 0.01$). Cell nuclear alignment and aspect ratio were also increased on elongated micro-scale boundary conditions (Fig. 3C), with nuclear aspect ratio 50% higher than cells on square patterns. Fibrillar collagen organization was also greatly enhanced on high aspect ratio patterns, with polarized light and SHG imaging revealing highly aligned fibrillar collagen (Fig 3D). Polarized light intensities were significantly greater for cells on elongated (10:1) boundary conditions (Fig 3D, left), with a pronounced peak in polarized light intensity with changing polarizer angle indicating a high degree of fibril alignment. SHG FFT analysis confirmed fibrils were highly aligned in the pattern direction (Fig 3D, right), with SHG AI values significantly higher than square (1:1) patterns (not shown, 3.19 ± 0.10 vs. 1.82 ± 0.09, $p < 0.0001$, $n = 3–4$ per condition). To investigate whether these observed differences were due to the difference in overall pattern length, we incrementally extended the meso-scale pattern boundary in one dimension (Fig 3E, 250 μm increments, aligned micro-scale pattern) and measured cell and fibrillar collagen organization (12 days of culture, $n = 4$ patterns per condition). Fibrillar collagen content and alignment was found to increase with increasing meso-scale length (Fig 3E, bottom left), including a large increase when pattern length was extended from 500 to 750 microns (2.38-fold increase in mean pixel intensity at polarizer angle = 40°; 2.49-fold increase in area-under-curve). Similarly, cell nuclear aspect ratios also were found to increase with increasing pattern length (Fig. 3E, $p < 0.001$, $r^2 = 0.174$). Together, these results illustrate that meso-scale boundary cues combine with micro-scale cues to dramatically affect cell and fibrillar collagen organization and alignment.

3.3. Opposed micro- and meso-scale cues compete to direct cell organization

To further examine the interaction between architectural cues at different length scales, we created μPP architectures with aligned micro-scale (as described above) and meso-scale (1250 μm × 125 μm pattern boundary) cues arranged in opposing directions, as shown in Fig. 4A. hMSCs cultured on these patterns were found to align with the micro-pattern direction initially (30 min, Fig. 4B left), then over the next 24 h of culture reorient to become aligned with the micro-pattern direction (Fig. 4B right, Supplementary movie S1), indicating cell organization was predominantly controlled by meso-scale cues in this pattern configuration. We then investigated at what point meso-scale architectural cues ceased to dominate over micro-scale cues by creating a series of patterns with incrementally increasing meso-scale "*y*" dimensions, as shown in Fig. 4C. Following 3 days of culture,

hMSC actin cytoskeletal orientation was aligned with the meso-scale long-axis for patterns with the highest meso-scale aspect ratios (Fig. 4C top, y = 250 μm), showed no preferred orientation for patterns with a slightly larger y dimension (Fig. 4C middle, y = 500 μm), and then aligned with the micro-pattern direction as the y-dimension was further increased (Fig. 4C bottom, y = 750 μm). We measured cytoskeletal alignment over a range of meso-scale boundary conditions for both aligned and gridded micro-scale architectures (n = 3–5 per pattern condition, 3 days culture), as shown in Fig. 4D (meso-scale aspect ratios less than one (e.g. 1:10) indicate micro/meso cues oriented in opposing directions). For hMSCs cultured on aligned micro-pattern architecture (Fig 4D, blue line), actin alignment shifted from meso-scale alignment (low AI values) to micro-scale alignment (AI values above 1.0) as the meso aspect ratio was increased from 1:10 (AI = 0.23 ± 0.03) to 1:1 (AI = 2.41 ± 0.35), and increased further as meso aspect ratios further increased (10:1, AI = 3.25 ± 0.10). In contrast, hMSCs on grid micro-pattern architecture (Fig 4D, red line) showed significantly lower alignment (compared to aligned micro-architecture) for intermediate meso boundary aspect ratios (e.g. AI = 1.13 ± 0.36 for 1:1 meso boundary, $p < 0.05$), but matched alignment levels of aligned micro-architecture at very low (1:10) and high (10:1) meso aspect ratios, indicating meso-scale cues were dominant in these conditions.

Supplementary video related to this article can be found at http://dx.doi.org/10.1016/j.biomaterials.2014.08.047.

To investigate whether this dominance of meso-scale boundary cues was dependent upon cell–cell interactions, we cultured hMSCs at different cell densities on patterns with opposed micro/meso cues (Fig 4E, aligned micro-scale architecture, 250 μm × 1250 μm meso-scale boundary) and evaluated cell alignment (cell nuclear orientation) following 24 h of culture. Cells were seeded at low and high densities (1000 and 18,000 cells/cm^2, respectively), with cells on low seeding density patterns further categorized as “low” (≤3 cells in contact) or “medium” (>3 cells in contact) density. We found that cells at low density had nuclei oriented in the micro-pattern direction (Fig 4E, left), whereas cells at medium (Fig 4E, middle) and high densities (Fig 4E, right) had nuclei more aligned with meso-direction ($p < 0.01$, difference with low density distribution, Kolmogorov–Smirnov test), indicating that this meso-scale dominance is dependent on cell density. Together, these findings demonstrate that architectural cues at micro- and meso-length scales may compete with each other to control alignment outcomes, with (in some cases) meso-scale cues dominating over micro-scale cues via a cell density-dependent mechanism.

3.4. μPP architectural cues do not alter expression of key tendon and matrix genes

Finally, we investigated whether the large differences in fibrillar collagen content and organization observed between μPP architectural conditions coincided with changes in the expression of important collagen and tendon-related genes. hMSCs were cultured on μPP substrates with three different meso/micro-pattern architectures (as shown in Fig. 5) for 6–12 days, with gene expression (relative to unseeded Day 0 cells) assessed via quantitative RT-PCR. For type III collagen, a key component of immature collagen fibrils in developing tendon [43], expression was significantly increased on patterns with elongated meso-scale boundaries (10:1 aligned) compared to the same aligned micro-pattern with square

boundaries (1:1 aligned), as shown in Fig. 5, whereas (1:1 grid) exhibited intermediate expression levels. Expression levels for type I collagen, the major constituent of mature collagen fibrils in tendon [43], were found to increase over time in culture (Fig. 5, $p < 0.002$), but no differences in expression were detected between μPP pattern conditions. Similarly, levels of tenascin-c, an extracellular matrix glycoprotein present in tendon [44] increased with time but showed no differences between pattern architectures. Finally, the tendonspecific transcription factor scleraxis [23] showed no differences with time or between pattern architectures, although levels were ~3-fold higher compared to unseeded (control) cells. Overall, these findings suggest that the substantial differences in fibrillar collagen content and organization observed between pattern architectural conditions do not correspond with differences in gene expression for key matrix and tendon genes.

4. Discussion

Tissue microenvironments provide architectural cues that direct a variety of cell behaviors including cell shape, alignment, migration, and resulting tissue formation. In this study, we investigated the response of hMSC multicellular populations to combinations of cell-adhesive architectural cues at two distinctly different length scales (micro-scale ‘fibril-like’ architecture, meso-scale geometric confinement). We examined a range of cue combinations in order to gain a more comprehensive understanding of how the different length scales interact to direct multicellular organization, as well as fibrillar collagen content and alignment, outcomes with critical functional significance for aligned musculoskeletal tissues. We found that aligned cues at the “micro-scale” (~1–2 μm) were sufficient to direct hMSC cell shape, alignment, and resulting fibrillar collagen matrix deposition. However, when larger “meso-scale” (~100–1000 μm) geometric confinement cues were superimposed in alignment with the micro-cues, cell alignment and fibrillar collagen content were enhanced. Conversely, when cues at the two length scales were arranged orthogonally, they competed against each other to control final neo-tissue organization. These meso-scale cues dominated over the micro-scale as meso boundary aspect ratios were increased (lateral boundary dimensions reduced) and was cell-density-dependent, indicating that cell–cell interactions play a key role in determining these tissue organizational outcomes. These findings suggest that cues at multiple length scales are important in guiding and maintaining aligned tissue organization, but exhibit complex interactions that have complementary or competing roles in this process.

Cell-adhesive μPP micro-scale cues alone were found to direct hMSC behaviors including cell shape (elongation), actin cytoskeletal alignment, cell nucleus shape and nuclear alignment, both for single cells (Fig. 1) and groups of cells (Fig. 2). Additionally, these micro-scale cues were shown to affect assembly and organization of an aligned fibrillar collagen matrix (Fig. 2), which is critical to providing mechanical strength in variety of fibrous tissues including tendon. However, when hMSCs were confined within a limited, meso-scale space without orientation (250 μm square micro-scale boundaries), differences between micro-scale architectures (aligned, grid, and unpatterned) and the degree of alignment (AI values) on aligned architectures were relatively modest. In contrast, when meso-scale boundaries with high aspect ratios were aligned with micro-scale cues (10:1, Fig. 3), large increases in cell alignment and fibrillar collagen content and alignment were

observed. There are several factors that may contribute to this observed increase in cell and tissue alignment: first, lateral confinement cues from meso-scale boundaries (i.e. edges) may act to reinforce (or override) micro-alignment cues as migrating cells are restricted by or align with the pattern edge. Second, the extended long-axis dimension of the 10:1 meso-scale boundary (1250 μm, as compared to 250 μm for 1:1 boundary) permitted end-to-end cell arrangements where cell-generated tension could be transmitted along the length of the neo-tissue via cell–cell or cell-matrix interactions. This phenomenon was evidenced by increased actin cytoskeletal alignment (Fig 3B) and highly elongated cell nuclei (Fig 3C) for patterns with 10:1 meso-scale boundaries. Additionally, as the meso-scale boundary was incrementally extended in one direction (Fig 3E), the nuclear aspect ratio increased with increasing pattern length, also suggesting increased cell-generated tension and/or the alignment of tensional forces in this arrangement. This end-to-end cellular arrangement is also likely critical for assembly and alignment of fibrillar collagen: in an *in vitro* model of developing tendon-like tissue, assembling collagen fibrils are observed to pass from an originating cell to other cells along the length of the tissue (with some fibrils over 500 μm in length), and this assembly has been shown to be myosin-II tension dependent [45,46]. Correspondingly, we found that levels of fibrillar collagen increased as we extended meso-scale boundary length, with a large increase when pattern length surpassed 500 μm (Fig 3E). Together, these findings emphasize that while micro-scale aligned cues have demonstrable effects on cell and matrix alignment, meso-scale cues that provide lateral directional confinement (via oriented meso-scale boundaries) and permit longitudinal end-to-end arrangement of cells were critical to producing fibrillar collagen and highly aligned tissue constructs.

On patterns where micro- and meso-scale aligned cues were arranged in opposition (orthogonally, Fig. 4), hMSCs were observed to initially spread and align along micro-scale cues; however, by 12 h post-seeding cell orientation began to rotate and align with meso-scale cues (Fig 4B, Movie S1), with this alignment persisting for the duration of culture. This experiment highlights the contribution of cues at both length scales and demonstrates that when opposed, cues compete against each other to control tissue organization. To investigate the cellular mechanism underlying this meso-scale dominance, we seeded cells at varying densities and found that reorientation only occurred at higher cell densities (Fig 4E). This finding suggests that the dominance of meso-scale cues is dependent upon cell–cell interactions, which could be active (i.e. receptor-based) or passive (i.e. volume exclusion-based) in nature. Active cell–cell behaviors could involve aggregate forces of the cell group (cell-generated tension transferred via cell–cell (e.g. cadherin) or cell-matrix (e.g. integrin) interactions) being focused along the aggregate's long-axis, pulling cells and matrix fibrils into alignment) [47,48]. Alternatively, recent evidence suggests that cell migration in dense cell populations may be driven by volume exclusion mechanisms (mechanical exclusion due to cell incompressibility within the collective system, independent of cell tension or cell–cell junctions) [49,50], with cooperative cell movements observed above a threshold cell density [51]. In our study, the meso-pattern boundary edges form an oriented confinement cue that may act to "funnel" cell movements and alignment in a preferred direction; alternatively, the boundary edge could act as a very strong alignment cue whose effects are transferred laterally through adjacent cells in a non-autonomous fashion [50]. However, we observed

that the boundary effect of a single edge does not appear to be particularly strong, since in areas of larger square patterns (1250 μm × 1250 μm, aligned micro-cues) where a boundary edge was perpendicular to micro-cues, the effect of the micro-boundary on cell alignment could be detected over a distance of 1–2 cell lengths (~100–150 microns, Supplemental Fig. 1). In contrast, when boundaries were given a meso-scale orientation, they exhibited alignment effects over somewhat larger length scales: for patterns with opposed micro/meso alignment cues, meso cues negated the effect of aligned micro-cues at dimensions of 500 μm (Fig 4C), and dominated over them when the minor axis pattern dimension was reduced further; for patterns with grid micro-cues (no micro-scale alignment cue), meso cues had an effect over similar or even larger length scales (Fig 4D).

The dimension range where meso-scale cues were observed to control tissue organization corresponds to findings of other studies, and also may relate to the hierarchical structure found in various aligned tissues. In a recent study, Duclos and colleagues [8] showed that elongated fibroblast cells (NIH 3T3) cultured to confluence exhibit aligned domains with a typical dimension (orientation correlation length) of ~500 μm, and when cultured on adhesive stripes of varying widths, cells were found to be perfectly aligned in the direction of the stripe for widths smaller than the orientation correlation length. Similarly, Chou and colleagues [52] found that when hMSCs were cultured on cross-linked collagen substrates with imprinted channel topographies (channel widths 25–1000 μm), cell alignment and construct tensile properties (elastic modulus, ultimate strength) were significantly increased when channels were less than 500 μm in width. We note that a common feature of various highly-aligned tissues (tendon, ligament, muscle) is a hierarchical structure featuring fascicular units (surrounded by a boundary-forming sheath of connective tissue) with diameters on a scale similar to the micro-scale boundaries identified in this study. In tendon, fascicular diameters range from 50 to 400 μm, and this maximum fascicular dimension (~400 μm) is conserved across a variety of species and tissue sizes, from mouse [53] to horse [54]. Our findings suggest that this is the same length scale where meso-scale features exert a dominant effect on cell and tissue alignment, raising the possibility that one function of fascicular boundaries is to promote and maintain cell and tissue alignment, and that their diameter represents a characteristic dimension over which they have influence.

Our findings of dramatic differences between fibrillar collagen content and organization for cells cultured on differing μPP architectures led us to investigate whether these differences corresponded with changes in collagen or other tendon-related genes. On μPP architecture that produced the greatest amounts of highly-aligned fibrillar collagen (10:1 aligned), we found a significant, though modest (29%–56%) increase in expression of type III collagen mRNA relative to patterns with the same (aligned) micro-architecture but square meso-boundaries (1:1 aligned), as shown in Fig. 5, while patterns with square meso-boundaries and micro-scale gridded architecture (1:1 grid) had intermediate type III expression levels. As type III collagen is a component of immature, small-diameter fibrils in developing tendon [43], this increase could be related to the production of new collagen fibrils as these neo-tissues assemble. However, for several other key matrix constituents (type I collagen, tenascin-c) important in aligned fibrous tissues, no differences in gene expression levels were observed between pattern architectures (Fig. 5), although expression did increase with time. Additionally, the transcription factor scleraxis, expressed in developing tendon [23],

showed no differences with pattern architecture or time. These findings indicate that observed differences in fibrillar collagen do not follow large across-the-board changes in key matrix and tendon development genes, suggesting that the observed effects are post-translational in nature. One possible explanation is that observed differences in fibrillar collagen between pattern architectures are a result of cells' ability to assemble and organize collagen into fibrils, which is likely dependent upon cell alignment and organization, rather than changes in collagen or tendon-related gene or protein expression. This behavior is consistent with previous work showing that hMSCs deposited greater amounts of collagen protein in response to dynamic stretch, despite no change in collagen gene expression [55]. Alternatively, differences in fibrillar collagen could also be a result of post-transcriptional changes that affect protein expression: for example, contact guidance cues have been shown to alter hMSC micro-RNAs that control collagen expression [19]. A more comprehensive gene expression study examining a wider panel of genes would likely yield further insight into the phenotypic changes that occur as a result of microenvironment architecture. Overall, our present findings suggest a process where physical signals such as microenvironment architecture may affect fibril collagen assembly independently of major changes in collagen or tendon-related gene expression.

5. Conclusions

In summary, our findings demonstrate that combinations of architectural cues at different length scales regulate aligned neo-tissue formation by hMSCs in a complex and interactive manner. Cues at both micro- (~1–2 μm) and meso-scales (~100–1000 μm) can direct cell and fibrillar collagen organization, with maximum alignment observed in cases where aligned cues at both length scales were combined. In contrast, when opposed, micro- and meso-scale aligned cues were found to compete to control tissue organization. Meso-scale cues dominance was cell-density-dependent and controlled neo-tissue alignment for widths less than 500 μm, a dimension similar to that of fascicular boundaries present in tendon, muscle, and other aligned tissues. This finding suggests that fascicle structure could play a key role in guiding and maintaining tissue alignment and may have implications for tissue engineering strategies, where scaffold designs that incorporate cues at multiple length scales could improve neo-tissue organization and resulting functional outcomes [56]. Overall, our findings highlight the importance of guidance cues at multiple length scales and illustrate how each may contribute to formation and maintenance of aligned fibrous tissues.

Supplementary Material

Refer to Web version on PubMed Central for supplementary material.

Acknowledgments

This study was supported in part by Synthes USA (unrestricted fellowship), NIH grants AR065888, AR059784, AR065764, AG15768, AR48182, AR50245, AR48852, and AG46927. The authors thank Dan Sykora for help with image analysis and Dr. Holly Leddy for help with statistical analyses.

References

[1]. Richardson SH, Starborg T, Lu Y, Humphries SM, Meadows RS, Kadler KE. Tendon development requires regulation of cell condensation and cell shape via cadherin-11-mediated cell-cell junctions. Mol Cell Biol. 2007; 27:6218–28. [PubMed: 17562872]

[2]. Guilak F, Cohen DM, Estes BT, Gimble JM, Liedtke W, Chen CS. Control of stem cell fate by physical interactions with the extracellular matrix. Cell Stem Cell. 2009; 5:17–26. [PubMed: 19570510]

[3]. Kshitiz, Park J, Kim P, Helen W, Engler AJ, Levchenko A, et al. Control of stem cell fate and function by engineering physical microenvironments. Integr Biol (Camb). 2012; 4:1008–18. [PubMed: 23077731]

[4]. Baker BM, Shah RP, Silverstein AM, Esterhai JL, Burdick JA, Mauck RL. Sacrificial nanofibrous composites provide instruction without impediment and enable functional tissue formation. Proc Natl Acad Sci U S A. 2012; 109:14176–81. [PubMed: 22872864]

[5]. Burdick JA, Anseth KS. Photoencapsulation of osteoblasts in injectable RGD-modified PEG hydrogels for bone tissue engineering. Biomaterials. 2002; 23:4315–23. [PubMed: 12219821]

[6]. DeForest CA, Anseth KS. Advances in bioactive hydrogels to probe and direct cell fate. Annu Rev Chem Biomol Eng. 2012; 3:421–44. [PubMed: 22524507]

[7]. DeLong SA, Moon JJ, West JL. Covalently immobilized gradients of bFGF on hydrogel scaffolds for directed cell migration. Biomaterials. 2005; 26:3227–34. [PubMed: 15603817]

[8]. Duclos G, Garcia S, Yevick HG, Silberzan P. Perfect nematic order in confined monolayers of spindle-shaped cells. Soft Matter. 2014; 10:2346–53. [PubMed: 24623001]

[9]. Petrie TA, Raynor JE, Dumbauld DW, Lee TT, Jagtap S, Templeman KL, et al. Multivalent integrin-specific ligands enhance tissue healing and biomaterial integration. Sci Transl Med. 2010; 2:45ra60.

[10]. Baranski JD, Chaturvedi RR, Stevens KR, Eyckmans J, Carvalho B, Solorzano RD, et al. Geometric control of vascular networks to enhance engineered tissue integration and function. Proc Natl Acad Sci U S A. 2013; 110:7586–91. [PubMed: 23610423]

[11]. Leslie-Barbick JE, Shen C, Chen C, West JL. Micron-scale spatially patterned, covalently immobilized vascular endothelial growth factor on hydrogels accelerates endothelial tubulogenesis and increases cellular angiogenic responses. Tissue Eng Part A. 2011; 17:221–9. [PubMed: 20712418]

[12]. Dickinson RB, Guido S, Tranquillo RT. Biased cell migration of fibroblasts exhibiting contact guidance in oriented collagen gels. Ann Biomed Eng. 1994; 22:342–56. [PubMed: 7998680]

[13]. Dunn GA, Heath JP. A new hypothesis of contact guidance in tissue cells. Exp Cell Res. 1976; 101:1–14. [PubMed: 182511]

[14]. Nelson CM, Jean RP, Tan JL, Liu WF, Sniadecki NJ, Spector AA, et al. Emergent patterns of growth controlled by multicellular form and mechanics. Proc Natl Acad Sci U S A. 2005; 102:11594–9. [PubMed: 16049098]

[15]. Nelson CM, Vanduijn MM, Inman JL, Fletcher DA, Bissell MJ. Tissue geometry determines sites of mammary branching morphogenesis in organotypic cultures. Science. 2006; 314:298–300. [PubMed: 17038622]

[16]. Gallant ND, Charest JL, King WP, Garcia AJ. Micro- and nano-patterned substrates to manipulate cell adhesion. J Nanosci Nanotechnol. 2007; 7:803–7. [PubMed: 17450836]

[17]. Kolind K, Leong KW, Besenbacher F, Foss M. Guidance of stem cell fate on 2D patterned surfaces. Biomaterials. 2012; 33:6626–33. [PubMed: 22748769]

[18]. Kulangara K, Yang Y, Yang J, Leong KW. Nanotopography as modulator of human mesenchymal stem cell function. Biomaterials. 2012; 33:4998–5003. [PubMed: 22516607]

[19]. Yim EK, Darling EM, Kulangara K, Guilak F, Leong KW. Nanotopography-induced changes in focal adhesions, cytoskeletal organization, and mechanical properties of human mesenchymal stem cells. Biomaterials. 2010; 31:1299–306. [PubMed: 19879643]

[20]. Clark P, Connolly P, Curtis AS, Dow JA, Wilkinson CD. Topographical control of cell behaviour. I. Simple step cues. Development. 1987; 99:439–48. [PubMed: 3653011]

[21]. Chen CS, Mrksich M, Huang S, Whitesides GM, Ingber DE. Geometric control of cell life and death. Science. 1997; 276:1425–8. [PubMed: 9162012]

[22]. Dalby MJ, Riehle MO, Yarwood SJ, Wilkinson CD, Curtis AS. Nucleus alignment and cell signaling in fibroblasts: response to a micro-grooved topography. Exp Cell Res. 2003; 284:274–82. [PubMed: 12651159]

[23]. Wojciak-Stothard B, Madeja Z, Korohoda W, Curtis A, Wilkinson C. Activation of macrophage-like cells by multiple grooved substrata. Topographical control of cell behaviour. Cell Biol Int. 1995; 19:485–90. [PubMed: 7640662]

[24]. Flemming RG, Murphy CJ, Abrams GA, Goodman SL, Nealey PF. Effects of synthetic micro- and nano-structured surfaces on cell behavior. Biomaterials. 1999; 20:573–88. [PubMed: 10213360]

[25]. Moffat KL, Kwei AS, Spalazzi JP, Doty SB, Levine WN, Lu HH. Novel nanofiber-based scaffold for rotator cuff repair and augmentation. Tissue Eng Part A. 2009; 15:115–26. [PubMed: 18788982]

[26]. Yin Z, Chen X, Chen JL, Shen WL, Hieu Nguyen TM, Gao L, et al. The regulation of tendon stem cell differentiation by the alignment of nanofibers. Bio-materials. 2010; 31:2163–75.

[27]. Chainani A, Hippensteel KJ, Kishan A, Garrigues NW, Ruch DS, Guilak F, et al. Multilayered electrospun scaffolds for tendon tissue engineering. Tissue Eng Part A. 2013; 19:2594–604. [PubMed: 23808760]

[28]. Barber JG, Handorf AM, Allee TJ, Li WJ. Braided nanofibrous scaffold for tendon and ligament tissue engineering. Tissue Eng Part A. 2011; 19(11-12):1265–74. [PubMed: 21895485]

[29]. Klumpers DD, Mao AS, Smit TH, Mooney DJ. Linear patterning of mesenchymal condensations is modulated by geometric constraints. J R Soc Interface. 2014; 11:20140215. [PubMed: 24718453]

[30]. Gomez EW, Chen QK, Gjorevski N, Nelson CM. Tissue geometry patterns epithelial-mesenchymal transition via intercellular mechanotransduction. J Cell Biochem. 2010; 110:44–51. [PubMed: 20336666]

[31]. Raghavan S, Nelson CM, Baranski JD, Lim E, Chen CS. Geometrically controlled endothelial tubulogenesis in micropatterned gels. Tissue Eng Part A. 2010; 16:2255–63. [PubMed: 20180698]

[32]. Gjorevski N, Nelson CM. Mapping of mechanical strains and stresses around quiescent engineered three-dimensional epithelial tissues. Biophys J. 2012; 103:152–62. [PubMed: 22828342]

[33]. Ruiz SA, Chen CS. Emergence of patterned stem cell differentiation within multicellular structures. Stem Cells. 2008; 26:2921–7. [PubMed: 18703661]

[34]. Li B, Li F, Puskar KM, Wang JH. Spatial patterning of cell proliferation and differentiation depends on mechanical stress magnitude. J Biomech. 2009; 42:1622–7. [PubMed: 19482284]

[35]. Li JY, Ho YC, Chung YC, Lin FC, Liao WL, Tsai WB. Preparation of micron/submicron hybrid patterns via a two-stage UV-imprint technique and their dimensional effects on cell adhesion and alignment. Biofabrication. 2013; 5:035003. [PubMed: 23714853]

[36]. Seunarine K, Curtis AS, Meredith DO, Wilkinson CD, Riehle MO, Gadegaard N. A hierarchical response of cells to perpendicular micro- and nanometric textural cues. IEEE Trans Nanobioscience. 2009; 8:219–25. [PubMed: 19278933]

[37]. Crouch AS, Miller D, Luebke KJ, Hu W. Correlation of anisotropic cell behaviors with topographic aspect ratio. Biomaterials. 2009; 30:1560–7. [PubMed: 19118891]

[38]. Lopez-Bosque MJ, Tejeda-Montes E, Cazorla M, Linacero J, Atienza Y, Smith KH, et al. Fabrication of hierarchical micro-nanotopographies for cell attachment studies. Nanotechnology. 2013; 24:255305. [PubMed: 23727615]

[39]. Doyle AD, Wang FW, Matsumoto K, Yamada KM. One-dimensional topography underlies three-dimensional fibrillar cell migration. J Cell Biol. 2009; 184:481–90. [PubMed: 19221195]

[40]. Bowles RD, Williams RM, Zipfel WR, Bonassar LJ. Self-assembly of aligned tissue-engineered annulus fibrosus and intervertebral disc composite via collagen gel contraction. Tissue Eng Part A. 2010; 16:1339–48. [PubMed: 19905878]

[41]. Garrigues NW, Little D, O'Conor CJ, Guilak F. Use of an insulating mask for controlling anisotropy in multilayer electrospun scaffolds for tissue engineering. J Mater Chem. 2010; 20:8962–8. [PubMed: 21072247]

[42]. Preibisch S, Saalfeld S, Tomancak P. Globally optimal stitching of tiled 3D microscopic image acquisitions. Bioinformatics. 2009; 25:1463–5. [PubMed: 19346324]

[43]. Birk DE, Mayne R. Localization of collagen types I, III and V during tendon development. Changes in collagen types I and III are correlated with changes in fibril diameter. Eur J Cell Biol. 1997; 72:352–61. [PubMed: 9127735]

[44]. Riley GP, Harrall RL, Cawston TE, Hazleman BL, Mackie EJ. Tenascin-C and human tendon degeneration. Am J Pathol. 1996; 149:933–43. [PubMed: 8780397]

[45]. Kalson NS, Starborg T, Lu Y, Mironov A, Humphries SM, Holmes DF, et al. Nonmuscle myosin II powered transport of newly formed collagen fibrils at the plasma membrane. Proc Natl Acad Sci U S A. 2013; 110:E4743–52. [PubMed: 24248360]

[46]. Kapacee Z, Richardson SH, Lu Y, Starborg T, Holmes DF, Baar K, et al. Tension is required for fibripositor formation. Matrix Biol. 2008; 27:371–5. [PubMed: 18262777]

[47]. Legant WR, Pathak A, Yang MT, Deshpande VS, McMeeking RM, Chen CS. Microfabricated tissue gauges to measure and manipulate forces from 3D microtissues. Proc Natl Acad Sci U S A. 2009; 106:10097–102. [PubMed: 19541627]

[48]. Stopak D, Harris AK. Connective tissue morphogenesis by fibroblast traction. I. Tissue culture observations. Dev Biol. 1982; 90:383–98. [PubMed: 7075867]

[49]. Angelini TE, Hannezo E, Trepat X, Marquez M, Fredberg JJ, Weitz DA. Glass-like dynamics of collective cell migration. Proc Natl Acad Sci U S A. 2011; 108:4714–9. [PubMed: 21321233]

[50]. Londono C, Loureiro MJ, Slater B, Lucker PB, Soleas J, Sathananthan S, et al. Nonautonomous contact guidance signaling during collective cell migration. Proc Natl Acad Sci U S A. 2014; 111:1807–12. [PubMed: 24449852]

[51]. Doxzen K, Vedula SR, Leong MC, Hirata H, Gov NS, Kabla AJ, et al. Guidance of collective cell migration by substrate geometry. Integr Biol (Camb). 2013; 5:1026–35. [PubMed: 23784144]

[52]. Chou CL, Rivera AL, Sakai T, Caplan AI, Goldberg VM, Welter JF, et al. Micro-meter scale guidance of mesenchymal stem cells to form structurally oriented cartilage extracellular matrix. Tissue Eng Part A. 2013; 19:1081–90. [PubMed: 23157410]

[53]. Derwin KA, Soslowsky LJ. A quantitative investigation of structure-function relationships in a tendon fascicle model. J Biomech Eng. 1999; 121:598–604. [PubMed: 10633259]

[54]. Thorpe CT, Udeze CP, Birch HL, Clegg PD, Screen HR. Capacity for sliding between tendon fascicles decreases with ageing in injury prone equine tendons: a possible mechanism for age-related tendinopathy? Eur Cell Mater. 2013; 25:48–60. [PubMed: 23300032]

[55]. Kuo CK, Tuan RS. Mechanoactive tenogenic differentiation of human mesenchymal stem cells. Tissue Eng Part A. 2008; 14:1615–27. [PubMed: 18759661]

[56]. Guilak F, Butler DL, Goldstein SA, Baaijens FPT. Biomechanics and mechanobiology in functional tissue engineering. J Biomech. 2014; 47:1933–40. [PubMed: 24818797]

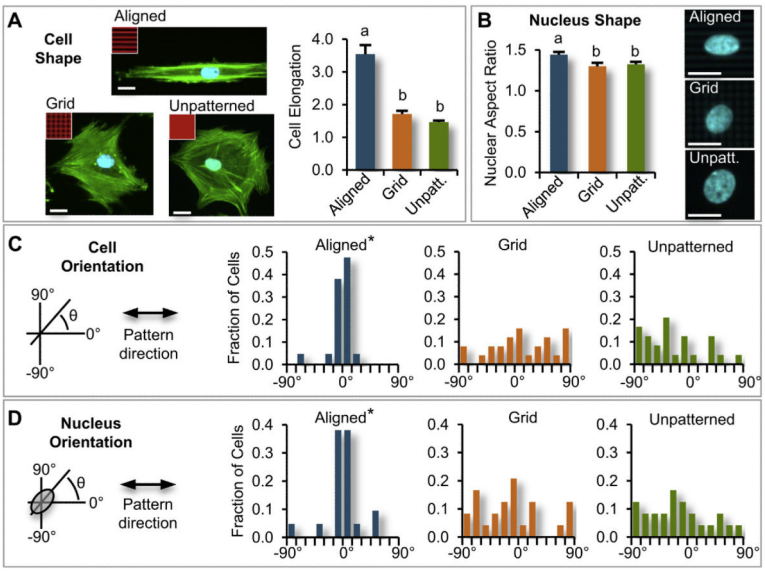

Fig. 1.

Micro-photopattern (μPP) micro-scale architecture directs alignment and shape of single hMSCs. (A) hMSCs were seeded on μPP substrates with aligned, grid, or unpatterned micro-scale cell-adhesive architectures (green:actin; blue:cell nuclei; red(inset):fluorescently-labeled fibronectin showing μPP architecture), with cell elongation (max/min Feret diameter) and cell nuclear aspect ratios measured following 2h attachment. Single hMSCs (not in contact with other cells) on aligned architectures were (B) more elongated (ANOVA, $p < 0.0001$, $n = 21–25$ cells/substrate condition, conditions labeled with different letters were statistically different) and (C) exhibited higher nuclear aspect ratios (ANOVA, $p < 0.01$) compared to cells on grid or unpatterned μPP architectures (representative images of cell nuclei shown on right). On aligned μPP architecture, cells (D) and cell nuclei (E) were significantly more aligned with pattern direction, in contrast to on grid or unpatterned architectures (*$p < 0.01$ compared to grid, unpatterned, Kolmogorov–Smirnov test). Scale bars = 20 μm. (For interpretation of the references to colour in this figure legend, the reader is referred to the web version of this article.)

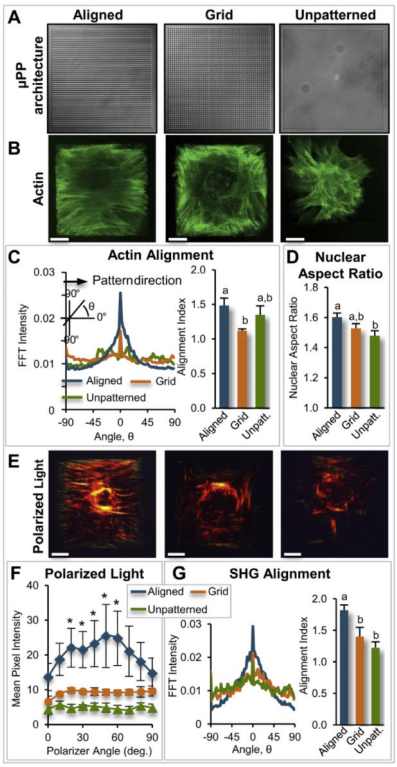

Fig. 2.

Micro-photopattern (μPP) micro-scale architecture directs hMSC multicellular organization and fibrillar collagen deposition. hMSCs were seeded at high density on μPP substrates (A) with aligned, grid, or unpatterned micro-scale cell-adhesive architectures and square (250 μm × 250 μm) meso-scale boundaries. Following 12 days culture, hMSCs on aligned μPP exhibited an aligned actin cytoskeleton (B), in contrast to cells on grid or unpatterned μPP architectures. FFT analysis of cytoskeletal organization (C) confirmed alignment with pattern direction, with significantly higher actin alignment index (AI, ANOVA, $p < 0.04$, $n = 4$, conditions labeled with different letters were statistically different) on aligned μPP relative to grid; cells on unpatterned μPP had intermediate AI levels due to local but randomly-oriented alignment of cell aggregates. hMSCs on aligned μPP had nuclei with higher aspect ratios than on unpatterned substrates (D, ANOVA, $p < 0.02$, $n = 56–81$ cells per condition, different letters were statistically different), with intermediate levels for cells on grid μPP. Polarized light imaging of fibrillar collagen (E) identified changes in polarized light intensities with polarizer angle (F) for aligned patterns (*difference between mean intensity and intensity at 0° polarizer angle for given pattern, $p < 0.05$), but not for grid or unpatterned substrates, demonstrating that aligned μPP architecture promotes aligned fibrillar collagen deposition. FFT analysis of SHG images (G, images not shown) confirmed alignment of fibrillar collagen with μPP architecture, with higher SHG alignment index (ANOVA, $p < 0.04$, $n = 4$, different letters were statistically different) on aligned relative to grid and unpatterned substrates. Scale bars = 50 μm.

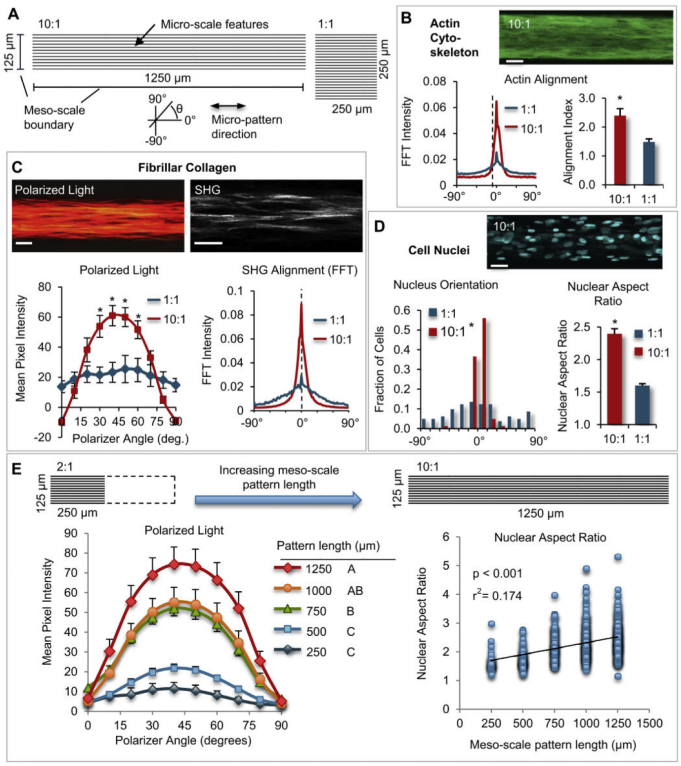

Fig. 3.

Aligned meso-scale architecture enhances cell and matrix organization. (A) hMSCs cultured on μPP substrates with high aspect ratio meso-scale boundary conditions aligned with micro-scale architecture (10:1 meso-scale aspect ratio) exhibit greater (B) actin cytoskeletal alignment with pattern direction as compared to cells on μPP substrates with square (1:1) boundaries (*t*-test, **p* = 0.014, *n* = 4) (C) The presence and organization of fibrillar collagen was also greatly enhanced for hMSCs cultured on μPP substrates with elongated (10:1) meso-scale boundary conditions as compared to patterns with 1:1 micro-scale boundaries. Polarized light intensities were significantly increased for 10:1 boundaries as compared to 1:1 boundaries (*difference between aspect ratios at given polarizer angle, $p < 0.05$, $n = 4–5$/condition). Fourier analysis of SHG images confirmed strong alignment with pattern direction, with a significantly higher collagen fiber alignment index for patterns with 10:1 boundaries (not shown, 3.19 ± 0.10 vs. 1.82 ± 0.09, $p < 0.0001$, $n = 3–4$ per condition). (D) Cell nuclei were also found to be more highly aligned with pattern direction relative to cells on 1:1 boundary substrates (*$p < 0.01$, Kolmogorov–Smirnov test), with nuclear aspect ratios significantly increased (*t*-test, *$p < 0.001$, $n = 81–82$ cells/condition). (E) When pattern aspect ratio was incrementally extended (250 μm increments resulting in increasing meso-scale aspect ratio), levels of aligned fibrillar collagen (left, polarized light, hMSCs cultured 12 days, conditions with different letters were significantly different for polarizer angles from 30° to 70°, ANOVA at each polarizer angle, $p < 0.05$, $n = 4$ per condition, one-sided error bars shown for clarity) and cell nuclear aspect ratios (right, linear fit, slope significantly greater than 0, $p < 0.001$, $n = 34–184$ cells per condition) increased with increasing pattern length. Scale bars = 50 μm.

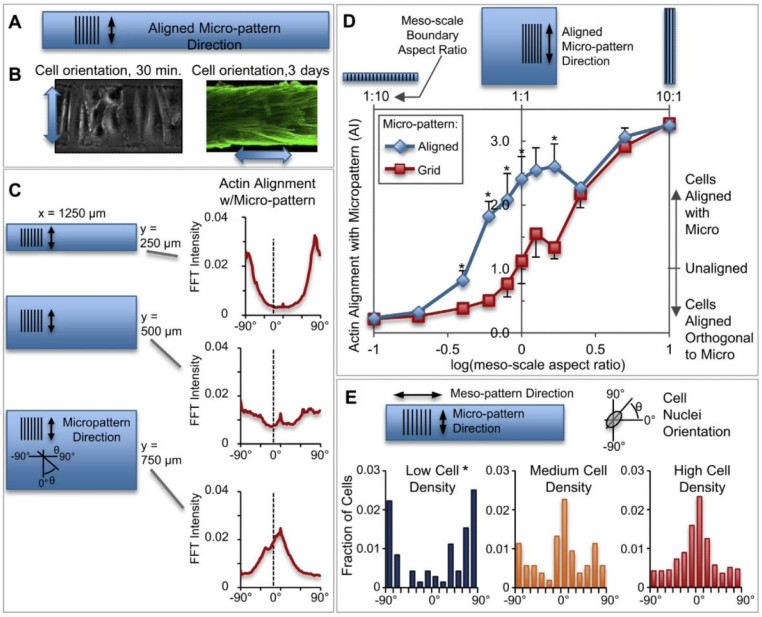

Fig. 4.

Opposed micro- and meso-scale architectures compete to direct hMSC organization, with meso-scale cues dominating via a cell density-dependent mechanism. (A) hMSCs seeded on μPP architectures with micro- and meso-scale cues arranged in opposing directions (micro-scale aligned pattern; meso-scale = 1:10 aspect ratio, 125 μm × 1250 μm pattern boundary) were found to initially align with the μPP micro-pattern direction (B, left, 30 min post-seeding), then over the next 1–3 days of culture reorient to become aligned with the meso-pattern direction (b, right, 3 days post-seeding, green = actin). (C) When hMSCs were cultured on μPP opposed architectures with increasing "short" (*y*-dimension) meso-scale boundary dimensions, cells on patterns with the smallest *y*-dimensions were found to align with the meso-direction (*y* = 250 μm, top, actin alignment, 3 days culture), showed no preferred orientation when *y* = 500 μm (middle), and aligned with micro-cues as *y* increased further (*y* = 750 μm, bottom). (D) hMSC actin alignment (alignment index, AI) was measured over a range meso-scale boundary conditions: on aligned micro-architecture (blue line), actin alignment shifted from meso (low AI values) to micro-alignment (high AI values) with increasing aspect ratio (*n* = 3–5 per pattern condition, 3d culture, one-sided error bars for clarity). On grid micro-architecture (red line), there was little actin alignment when the meso boundary aspect ratio was 1:1 (AI near 1), but AI values rapidly approached those of aligned micro-architecture as meso aspect ratios were increased (*$p < 0.05$, *t*-test, difference between micro-pattern (aligned, grid) at given meso-scale aspect ratio). (E) hMSCs seeded at low and high densities on patterns with opposed micro/meso cues (aligned micro-architecture, 1250 μm × 250 μm meso boundary, 24 h culture) were categorized as 'low' (≤3 cells in contact) or 'medium' (>3 cells in contact) cell densities. Cells at low density had nuclei oriented in the micro direction (left), whereas cells at medium (middle) and high (right) densities had nuclei more aligned with meso-direction (*$p < 0.01$ compared to medium and high cell densities, Kolmogorov–Smirnov test). (For interpretation of the references to colour in this figure legend, the reader is referred to the web version of this article.)

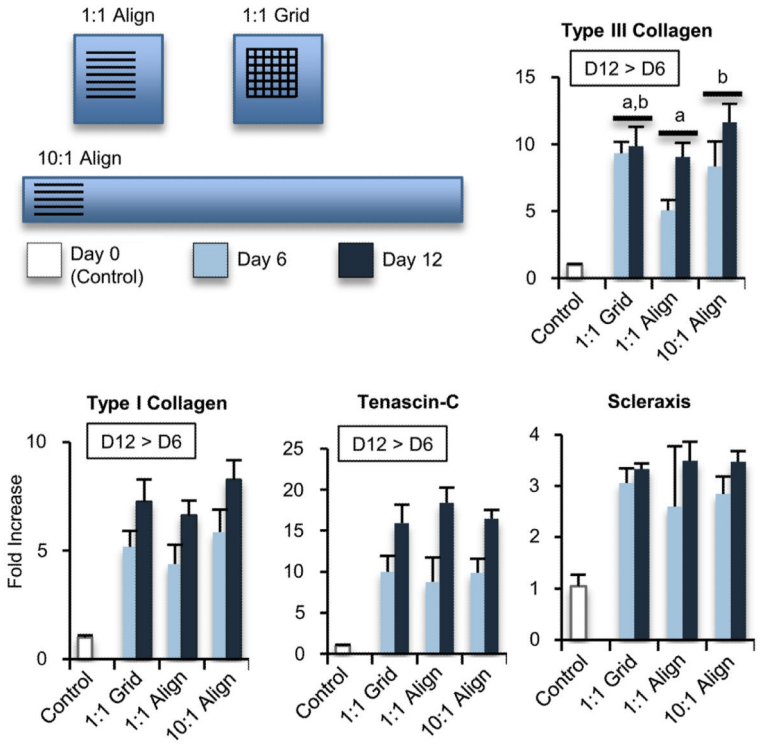

Fig. 5.

μPP architectural cues do not affect expression of key tendon and matrix genes. hMSCs were cultured on three different meso/micro μPP architectures (top; 1:1 aligned, 1:1 grid, 10:1 aligned) for 6 or 12 days, with gene expression levels (relative to unseeded Day 0 cells) assessed via quantitative RT-PCR (n = 3–4 per pattern condition, two-factor ANOVA (time, pattern)). Expression levels for type I collagen (COL1A1) and tenascin-c (TNC) were found to increase with time in culture (D12 > D6, $p < 0.002$ for COL1A1, $p < 0.0001$ for TNC), but no differences were detected between pattern conditions ($p = 0.14$ and $p = 0.93$, respectively). For type III collagen (COL3A1), expression was increased on patterns with elongated meso-scale boundaries (10:1 aligned) compared to the same aligned micro-pattern with square boundaries (1:1 aligned, $p = 0.043$, conditions labeled with different letters were statistically different), with cells on 1:1 grid patterns exhibiting intermediate expression levels. Levels of scleraxis (SCXB) showed no differences with time ($p = 0.08$) or between pattern architectures ($p = 0.93$), although levels were ~3-fold higher than control cells.